JOURNAL OF AEROSPACE COMPUTING, INFORMATION, AND COMMUNICATION
Vol. 1, July 2004

Noise-Sensitive Final Approach Trajectory Optimization for Runway-Independent Aircraft

Ella M. Atkins* and Min Xue†
University of Maryland, College Park, Maryland 20742

Runway-independent aircraft could increase passenger throughput at crowded urban airports via the use of vertiports or stub runways. Simultaneous non-interfering traffic procedures could minimize impact on existing fixed-wing traffic, and noise abatement procedures could minimize the impact of radiated noise to surrounding communities. This paper introduces a global optimization technique based on cell decomposition that automatically constructs simultaneous non-interfering noise abatement procedures for runway-independent aircraft. The objective function includes radiated ground noise, time, and fuel. The flight envelope is represented by search-space constraints, and fixed-wing traffic corridors are modeled as impenetrable obstacles. Baseline single-segment approach trajectories are compared with a suite of automatically generated routes to study the tradeoff between noise, fuel/time efficiency, and path complexity. Example final approach trajectories illustrate the effects of airspace obstacle placement, relative optimization function weights, and varied search-space discretization depth. This optimization tool will provide airport and airspace designers with a host of alterative trajectory options for analysis of potential landing sites and associated traffic procedures. The iterative deepening search strategy is also applicable as an anytime algorithm for real-time computation of low-noise routes around traffic or weather "obstacles".

Nomenclature

C_T	= thrust coefficient
c_i	= cost function weights
D	= helicopter drag
g	= gravitational constant
I_i, K_i, C_i	= BVI noise cost function coefficients
m_{fuel}	= total required fuel mass
SEL_{av}	= average Sound Exposure Level
SFC	= Specific Fuel Consumption (constant)
HP	= the power required per hour
P	= instantaneous ground noise
t	= time
t_0, t_f	= initial/final approach times
V	= flight velocity
$\dot{V}$	= acceleration
W	= helicopter weight
x	= lateral distance from landing site
y	= altitude
(x_f, y_f, V_f)	= final state boundary condition

Received 17 July 2003; revision received 30 November 2003; accepted for publication 21 April 2004.

*Senior Member, Assistant Professor, Department of Aerospace Engineering, 3182 Glenn L. Martin Hall; atkins@glue.umd.edu.
†Student Member, Graduate Research Assistant, Department of Aerospace Engineering, 1133 Manufacturing Building; minxue@glue.umd.edu.

(x_{min}, y_{min}, V_0) = approach entry constraints
$\alpha_{TPP,0}$ = tip-path-plane angle corresponding to zero miss distance
α_{TPP} = main rotor tip-path-plane angle
μ = advance ratio, ; W=rotor angular velocity, R=rotor radius
γ = flight path angle
γ_{min}, γ_{max} = min/max flight path angle constraints
$\dot{\gamma}$ = flight path angle rate of change

I. Introduction

THE National Airspace System must accommodate the increasing demand for commercial air transportation. In urban environments, runway real estate is limited and airspace bottlenecks form when traffic merges to final approach and departure corridors. Runway-independent aircraft (RIA) can increase passenger throughput by offloading short to medium-haul (<400nm) traffic from overcrowded runways, utilizing stub runways or vertiports as alternative landing sites. The RIA class includes vertical takeoff and landing (VTOL) and extremely short takeoff and landing (eSTOL) vehicles. High-capacity rotorcraft, tilt-rotor, and powered-lift fixed-wing RIA designs are being considered. Introduction of RIA traffic patterns in crowded terminal airspace has the potential to increase air traffic controller workload, creating new conflict-related delays rather than alleviating congestion. Simultaneous Non-Interfering (SNI) approach and departure procedures for RIA will minimize air traffic control overhead and maximize overall throughput.[1] SNI paths do not intersect existing traffic corridors, so RIA SNI arrivals and departures can be sequenced independent of fixed-wing traffic. By definition, SNI trajectories occupy previously unused airspace thus may overfly noise-sensitive communities previously undisturbed by fixed-wing traffic. As new SNI routes are proposed, public acceptance mandates the development of noise abatement procedures (NAP). RIA approach and departure routes must also be acceptable to pilots and air traffic controllers, comfortable for passengers, and economical for the airlines.

The following research tasks must be completed to define and implement viable terminal area traffic procedures for runway-independent aircraft:

1) Select candidate RIA design(s); build performance and noise models for these vehicles.

2) Define RIA final approach and takeoff (FATO) areas for each airport based on factors that include safety, airport architecture, ground operations (e.g., taxi routes), and air traffic flow.

3) Develop candidate NAPs that are efficient in time/fuel and that minimize radiated noise. SNI NAPs will minimize Air Traffic Control (ATC) coordination overhead but may increase flight path complexity to circumvent fixed-wing traffic corridors.

4) Assess desirability of each NAP with respect to efficiency (time/fuel), community noise exposure, safety, pilot preference, and ATC workload. RIA FATO area, fixed-wing traffic patterns, and ground noise constraints must all be identified to enable a comprehensive systems analysis of SNI NAPs at specific airports.

The goal of this research is to provide a segmented route optimization tool that enables rapid identification of acceptable NAPs as airport and airspace designers identify RIA landing sites and assess their impact on traffic and the surrounding communities. SNI routes are facilitated by approach and departure areas with few intersecting fixed-wing traffic corridors. Automatically-generated NAPs can be compared with the traditional single-segment trajectories typically preferred by pilots.[2] Our tool rapidly enables airport planners, controllers, and pilots to define and assess alternative trajectories with respect to cost (noise, time, fuel), providing solutions to be subsequently ranked in terms of pilot and ATC workload, impact on fixed-wing traffic, and safety.

This paper begins with an overview of the AH-1 rotorcraft performance and noise models used as the example RIA for this research. Next, a set of intuitive single-segment approaches are presented, illustrating the challenges associated with SNI NAP development for a powered-lift vehicle. A global optimization method using coupled modified cell decomposition and iterative deepening search algorithms is developed and applied to automatically generate a set of candidate low-cost SNI NAPs for final approach to landing. The search-space is designed to impose realistic constraints on aircraft flight path angle, velocity, and acceleration/deceleration. To find strictly SNI routes, existing fixed-wing traffic corridors are surrounded by a safe separation zone and modeled as impenetrable obstacles. Results are presented that illustrate how airspace obstacles, aircraft flight envelope limitations, and cost function elements influence final approach trajectory shape and corresponding velocity/acceleration profiles. The paper concludes with a discussion of future work to expand algorithm capabilities and deploy the SNI trajectory optimizer as a systems analysis tool that complements ongoing RIA vehicle design and airport planning efforts.

II. RIA Performance and Noise Models

Runway-independent aircraft are still in the concept stage with respect to both class (e.g., rotorcraft, tilt-rotor, eSTOL) and specific vehicle design characteristics. The SNI airspace model and optimization method presented in this work are general for any aircraft type. However, presented results are based on an AH-1 rotorcraft, enabling the use of experimentally validated performance and noise models for all optimization processes.

Flight plans are typically defined as a sequence of constant-velocity or constant-acceleration flight segments. To find trajectories well within both the AH-1 operating envelope and passenger comfort region, the following longitudinal plane dynamic constraints were imposed:

$$|\gamma| \le 9^{\circ},\ 38 \le V \le 105kts,\ |\dot{V}| \le 0.05g \tag{1}$$

where V is airspeed and g represents flight path angle. The optimization cost function includes time, fuel, and noise terms to enable efficient and quiet procedure designs. Time is directly computed from flight trajectory; fuel use up to time t_i is derived from a standard rotorcraft model:[3]

$$m_{fuel,i} = \sum_{k=1}^{i} SFC * HP_k * t_k \tag{2}$$

where SFC is Specific Fuel Consumption. HP_k is the power required per hour for flight segment k, and t_k is the corresponding time (in hours). HP_k can be expressed as:

$$HP_k = \rho A(\Omega R)^3 \left[\frac{kC_T^2}{2\mu} - \mu\alpha_{TPP}C_T + \frac{sC_{d0}}{8(1+4.6\mu^2)} \right] \tag{3}$$

where α_{TPP} = -D/W - γ, D is a function of (V – $f(V^2)$), and $\mu = V/(\Omega R)$. $\rho A(\Omega R)^3, C_T, s, C_{d0}$, and k can all be treated as rotorcraft model-specific constants during approach. Although engine power should include tail rotor power and installation losses, these are secondary effects and may be considered independent of flight condition in the longitudinal plane. Thus, given Eqs. (2) and (3), fuel consumption is a function of V and γ. For the AH-1 helicopter, the nominal power requirement is shown in Fig. 1.

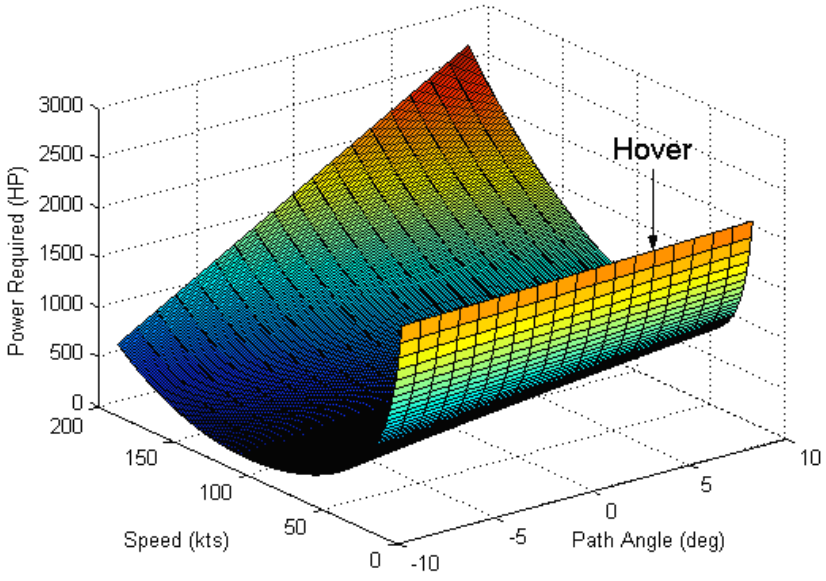

Fig. 1 AH-1 nominal power requirement.

For any rotorcraft or tilt-rotor after conversion to helicopter mode, the dominant noise source on approach is blade-vortex interaction (BVI). BVI has highest amplitude when the rotor disk passes directly through the vortex wake. Other noise sources (e.g., engine) are of increasing importance during departure, where maximum power is required and vortices are well below the rotor blades. BVI noise is the typical popping or slapping sound that radiates significant acoustic energy far from its source. For efficiency, this research utilizes an empirical aeroacoustics function $P(J_i, C_i, I_i, V, x, y)$, derived by Gopalan et al.[4] for impulsive (BVI) rotorcraft noise from the experimentally-verified Quasi-Static Acoustic Mapping (Q-SAM) approach:[5]

$$P(K_i,C_i,I_i,V_i,x,y) = K_1(1+\mu)^{K^2} + C_1 * 10\log_{10}\left(\log_{10}\left(1+\frac{C_2 A_0 (y_1/y)^5}{P}\right)\right) + C_3$$
$$\begin{cases} -20\log_{10}\left(1+I_1\mu^2\left(\alpha_{TPP,0}-\alpha_{TPP}\right)^2\right) \alpha_{TPP} < \alpha_{TPP,0} \\ -20\log_{10}\left(1+I_2\mu^2\left(\alpha_{TPP,0}-\alpha_{TPP}\right)^2\right) \alpha_{TPP} > \alpha_{TPP,0} \end{cases} \tag{4}$$

In Eq. (4), P refers to the average Sound Exposure Level (SELav) expressed in decibels (dB). I_i is a function of the advance ratio μ for a specific BVI, and the C_i and K_i are constants computed from a curve-fit of experimental trends. $\alpha_{TPP,0}$ is the rotor tip-path-plane angle corresponding to wake vortex zero miss distance and is a function of V. This empirical noise model represents the average sound power (SELav) radiated by the helicopter over a representative observer plane a distance y below the helicopter.[4] P is integrated over the flight trajectory from time t_0 to t_i to provide a single noise term in the objective function used for this work:

$$f_{noise} = \int_{t_0}^{t_i} 10^{P/10}\, dt \tag{5}$$

To gain insight into BVI behavior as a function of velocity, acceleration, and flight path angle, Fig. 2 illustrates typical BVI noise (P) for the AH-1 rotorcraft at four flight speeds ranging from 45 to 105 knots. Note the dependence of noise on flight path angle and the movement of a central ridge defining the peak noise region as velocity V is varied. This velocity dependence complicates the identification of acceptable accelerating/decelerating SNI NAPs as will be demonstrated next.

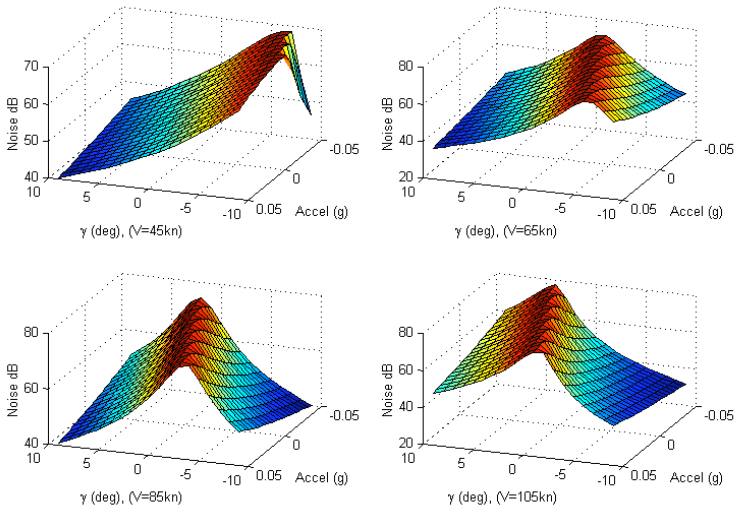

Fig. 2 BVI noise characteristics for the AH-1.

III. Single Segment RIA NAP Design

Pilot studies have indicated a simple one-segment final approach is preferred to a more complex segmented route.[2] This research also concluded that a decelerating three-degree approach significantly reduced fixed-wing aircraft noise, as was experimentally verified at the Louisville International Airport.[6] Engine thrust is a dominant noise source for fixed-wing aircraft, and a decelerating approach enables reduced thrust thus reduced noise. A departure climb requires significant thrust, so departure NAPs may require throttle cutbacks and lateral diversion around populated areas.[2] Results from a recent Boeing 747-400 flight simulation study[7] indicate that pilots found both vertically segmented and continuous [decelerating] descent strategies acceptable, but that workload was higher (moderate) with the vertically segmented NAP. Note that adoption of the decelerating descent approach strategy is contingent on the development of air traffic control automation aids, since staged aircraft may be decelerating at different rates and minimum separation must be maintained throughout the approach.[8]

To provide a baseline comparison between typical fixed-wing and potential RIA NAPs, Fig. 3 shows a set of single-segment approach trajectories with varied γ, V, and $\dot{V}$ values. Cases I-III depict three different velocity profiles along a standard 3° descent approach (γ = -3°), while Cases IV and V-VII utilize the same set of velocity profiles along 6° and 9° descent paths, respectively. Each approach begins at a lateral distance of 40000 ft (6.6nm) from the FATO area. Table 1 summarizes the noise (5), time, and fuel (2) requirements for each candidate NAP. Consider the 3° standard descent approach. As shown in Fig. 2, significant BVI noise occurs at mid-range velocities (60-90 knots) for shallow descent paths, resulting in high, integrated noise levels for Case I (V=70) and Case III (decelerating). Although Case II (V=45) radiates less noise, efficiency is poor, with over twice the fuel required to maintain the prolonged shallow descent.

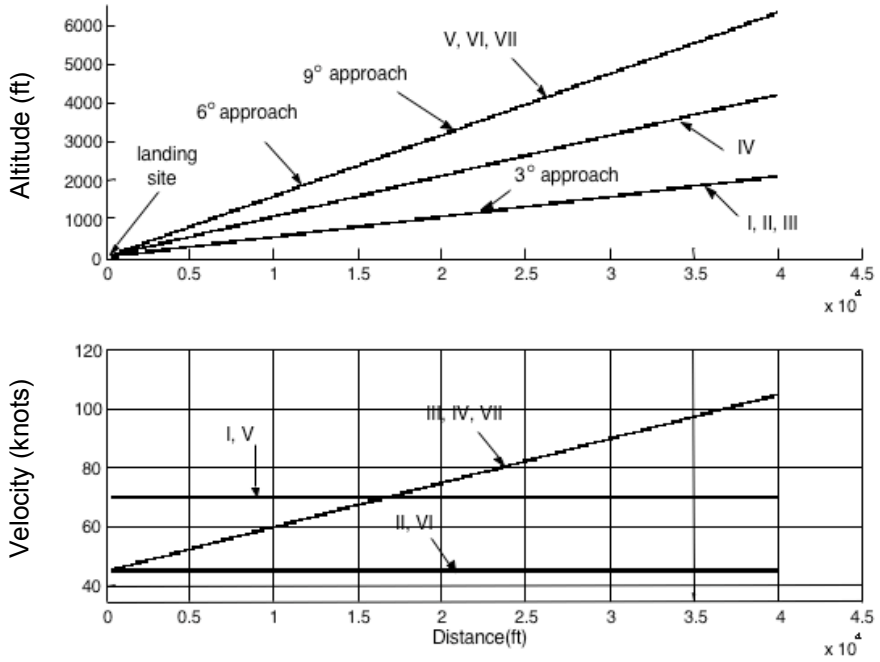

Fig. 3 Single-segment final approach trajectories.

The remaining cases illustrate the effects of increased descent path angle. The 6° decelerating descent (Case IV) shows only minor noise reduction relative to the 3° case, with some additional improvement observed for the decelerating 9° descent (Case VII). However, the higher velocity Case V (V=70) now radiates less noise than Case VI (V=45) since peak BVI noise for steep descent paths occurs at low velocities (Fig. 2). Overall, Table 1 suggests Case V, a 9° constant high-velocity descent, as the best single-segment solution. BVI noise is the lowest, and fuel efficiency is best with a steep descent path and moderate flight velocity. Two factors must be addressed before this solution can be implemented, however. First, the 70-knot velocity must be reduced prior to landing. Deceleration magnitude is limited by passenger comfort and safety considerations — pilots will not prefer to arrive at the FATO

area in a steep descent with extra energy. Second, the single-segment solution is only SNI if no fixed-wing airspace passes through this segment. The airspace optimization tool presented below automatically builds SNI paths and identifies low-noise procedures that meet specified boundary velocity constraints.

Table 1 Single Segment Approach Cost

Case	γ	$V(kt), \dot{V}(ft^2/s)$	BVI Noise *(SEL_{av})* (dB)	Time (s)	Fuel (lb)
I	-3°	$V = 70,\ \dot{V} = 0$	89.4	338.8	21.98
II	-3°	$V = 45,\ \dot{V} = 0$	81.8	527.1	46.85
III	-3°	$V_i = 105, V_f = 45,$ $\dot{V} = -0.01g$	92.8	317.6	21.45
IV	-6°	$V_i = 105, V_f = 45,$ $\dot{V} = -0.01g$	90.0	318.9	14.99
V	-9°	$V = 70,\ \dot{V} = 0$	***77.0***	***342.6***	***9.03***
VI	-9°	$V = 45,\ \dot{V} = 0$	89.6	532.9	34.2
VII	-9°	$V_i = 105, V_f = 45,$ $\dot{V} = -0.01g$	86.1	321.1	8.49

IV. Trajectory Optimization Algorithm

Much of the past work on automatic trajectory synthesis for aircraft has focused on generating continuous-space solutions that minimize fuel and time subject to airspace and air traffic control constraints. Betts[9] presents a thorough review of two-point boundary value problems with direct and indirect solution techniques. Seywald et al.[10] and Schultz[11] discuss trajectory optimization for aircraft flying in the longitudinal plane using a point mass performance model. Hagelauer[12] proposes an approach to flight path optimization based on dynamic programming, while Slattery and Zhao[13] synthesize trajectories for air traffic management so controllers can better guarantee safety and increase efficiency via minimal spacing.

Individual aircraft trajectories may be mathematically optimized, and existing autopilots with advanced navigation and control technologies are able to precisely follow complex optimal paths. However, *segmented routes* such as those computed by Vormer et al.[14] with a genetic algorithm (GA) enable intuitive comprehension by pilots and ATC, facilitate communication of trajectory, and typically reduce computational complexity relative to complex numerical global optimization processes. For this work, SNI final approach trajectory optimization is defined as a single-point (fixed FATO area) boundary value problem in the longitudinal plane, and noise abatement procedures are described by a sequence of one or more segments, each with constant velocity or acceleration. The approach entry point is constrained by minimum lateral distance (e.g., x=40000 ft) and altitude (e.g., y=2000 ft) so that the optimizer can then *define* the specific SNI NAP entry fix. The optimization algorithm must minimize cost (noise, time, fuel) in the presence of dynamic constraints and impenetrable airspace obstacles. Described by Latombe,[15] several techniques, including roadmap, potential field, and cell decomposition, exist for motion planning in obstacle fields. Most of these methods were developed for ground robots with few motion constraints, however the roadmap method using Voronoi diagrams has been extended for use during aircraft/UAV trajectory optimization.[16]

We have adopted a cell decomposition strategy for this work due to its ability to model arbitrary obstacles, guarantee globally-optimal results limited only by discrete cell size, and allow arbitrarily complex cost functions *f*. The approximate cell decomposition approach was first introduced by Lozano-Perez and Brooks[17] and has been utilized in varied forms by a number of researchers. Although typically more computationally complex than local techniques, optimal SNI airspace design benefits more from geometric and cost parameter flexibility than from real-time performance. The fundamental cell decomposition algorithm[15] is given as follows:

Let S (search space) be a rectangloid of R^m, where m is the search space dimension. A rectangloid decomposition of κ of S is a finite collection of rectangloids $\{\kappa_i\}_{i=1,2\cdots r}$, such that:

- S is equal to the union of the $\{\kappa_i\}$, i.e.: $S = \bigcup_{i=1}^{r} \kappa_i$, $i = 1,2\cdots r$.
- The interiors of the κ_i's do not intersect, i.e.: $\forall i_1, i_2 \in [1,r], i_1 \neq i_2 : \text{int}(\kappa_{i_1}) \cap \text{int}(\kappa_{i_2}) = \phi$

Each rectangloid κ_i is called a cell of the decomposition κ of S. Two cells are ***adjacent*** if and only if their intersection is a set of non-zero measure in R^{m-1}. A cell κ_i is classified as:

- EMPTY, if and only if its interior does not intersect the obstacle region.
- FULL, if and only if κ_i is entirely contained in the obstacle region
- MIXED, otherwise.

The ***connectivity graph*** G associated with a decomposition κ of S is defined as follows:

- Nodes of G are EMPTY and MIXED cells of κ.
- Two nodes of G are connected by a link if and only if corresponding cells are adjacent. In our case the link is a straight line connecting the centers of nodes.

Given a rectangloid decomposition, a *channel* is defined as a sequence $\left(\kappa_{a_j}\right)_{j=1,\cdots p}$ of EMPTY and/or MIXED cells such that any two consecutive cells κ_{a_j} and $\kappa_{a_{j+1}}, j \in [1, p-1]$ are adjacent. An ***E-channel*** contains only EMPTY cells, while an ***M-channel*** contains at least one MIXED cell. The most common technique used to build the space is to compute a 2^m-tree decomposition.

A. Modified Approximate Cell Decomposition

Basic cell decomposition focuses on obstacle avoidance and does not account for additional dynamic parameter constraints (e.g. velocity, acceleration, flight path angle). Modifications to the original algorithm have been made for this work such that constraints can be imposed during the optimization process. In the original case, with no obstacle, only one cell is generated, and the algorithm will have no results. This implies an obvious solution — a straight line between the initial and final states. However, the solution is not so trivial given dynamic constraints and our multi-parameter objective function, so to find an optimal path without obstacles empty cells are still divided. Given the definition of a decomposition algorithm, the trajectory will be composed of the links between centers of nodes. Cells by default have the aspect ratio of the overall map, and the [flight] path connects the centers of each cell. A square map yields square cells, which implies flight path angle choices [45˚, 0˚, -45˚] mandating level flight given our $|\gamma| \leq 9^\circ$ constraint. Cell length/width ratio can be used to control flight path angle resolution. For this work, the length:width ratio is set to 100:1, which yields a γ interval of ~ 0.6˚ as shown in Fig .4.

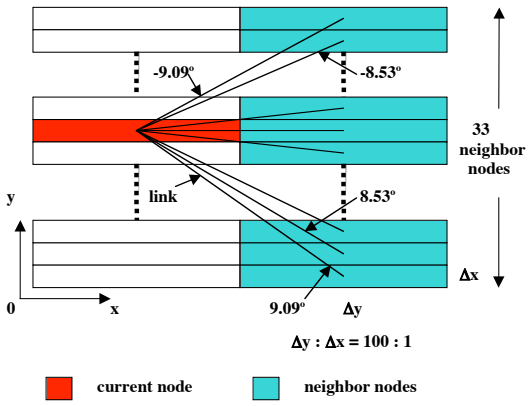

Fig. 4 Cell neighborhood illustrating flight path angle discretization.

Since a rotorcraft is assumed to climb or descend with a flight path angle between ±9˚, the concept of adjacent cells is expanded beyond standard "geometric" adjacency. Assuming the rotorcraft flies from right to left on the page, 33 nodes to the right of each cell (see Fig. 4) will be defined as adjacent (neighboring), yielding values $\gamma =$ ±9.09˚, ±8.53˚, ±7.97˚…±1.45˚, ±0.57˚, 0˚ for each step. With quad-tree decomposition, all cells maintain the same shape as in the original map. This two-dimensional longitudinal plane, the rootmap, is defined by a rectangle with maximum altitude and lateral distance as its width and length, respectively. The rootmap contains the approach entry region and FATO boundary (landing point) as cell centers, with the landing point defined as the *origin*. To meet the 100:1 *length:width* ratio requirement, the rootmap will be expanded either in length or width. Then, after the quad-

tree decomposition step, all cells whose center point is outside the rootmap space are dropped, while the cells with center point in the rootmap are used to construct the search space. Figure 5 shows an example modified cell decomposition with a single obstacle.

For existing acceleration constraints imposed primarily for passenger comfort considerations, $\left(-0.05g \le \dot{V} \le 0.05g\right)$, the range $38 \le V \le 105kts$ is divided into 20 intervals. Acceleration over a flight segment from node i to k is computed as $(V_k - V_i)/t$ providing a simple approximation to the continuous acceleration. To model the discrete velocity value set, each node will become 20 duplicate nodes with different velocities. If the total set of EMPTY nodes within the rootmap space is n, in the modified algorithm $20*33*n$ actual search nodes exist.

A final limitation of the original cell decomposition algorithm is that it does not make use of the information in MIXED cells. An optimal path may intersect the MIXED cells without intersecting the real obstacles. The modified cell decomposition algorithm allows the final path to enter the MIXED cells during traversal between two EMPTY cells so long as the path does not actually pass through the obstacle boundaries.

The flow chart for the modified cell decomposition strategy is shown in Fig. 6 and is driven by top-level procedure **Build**. In the figure, invariant data includes 'quad_depth', the maximum quad-tree depth level, and 'obstacles', the set of polygonal airspace obstacles. 'rootmap' is the top level geometric map to be decomposed into cells, 'map' represents a single geometric cell to [potentially] be divided, 'resolution' is the current tree depth (1=first decomposition step), and 'cells' is the list of all geometric cells. The 'quadrant' function returns a new cell representing one of the four subtrees (1, 2, 3, 4) of a rectangloid parent cell, the 'parent' function returns the parent cell, the 'position' function gives the subtree position of the cell with respect to its parent cell, and 'node' is a structure containing data for a geometric cell and corresponding velocity value. **BuildCell** is a recursive function to construct the geometric cell set and store the EMPTY cells that reside between the initial and final state 'rootmap' vertices to become search nodes. The set of nodes is constructed from cells and is defined by a (cell, velocity) pair plus a list of neighbor nodes. A node j is defined as a "reachable neighbor" of node i if it is geometrically adjacent and meets the γ and acceleration constraints.

Extensions to a three-dimensional cell map and three-dimensional validated noise model are required for full optimization over lateral and longitudinal motion. Previous fixed-wing NAP designs[2] have utilized lateral motion to divert around populated areas or follow procedures developed for ground-based navigation aids (e.g., VOR). New RIA operations will not inherit legacy procedures, and pilots will likely not prefer extended turns during final approach. However, as specific landing sites and noise-sensitive regions are identified, the modified cell concept can be extended to three-dimensional, defining cell dimensions that guarantee sufficient resolution in heading as well as flight path angle.

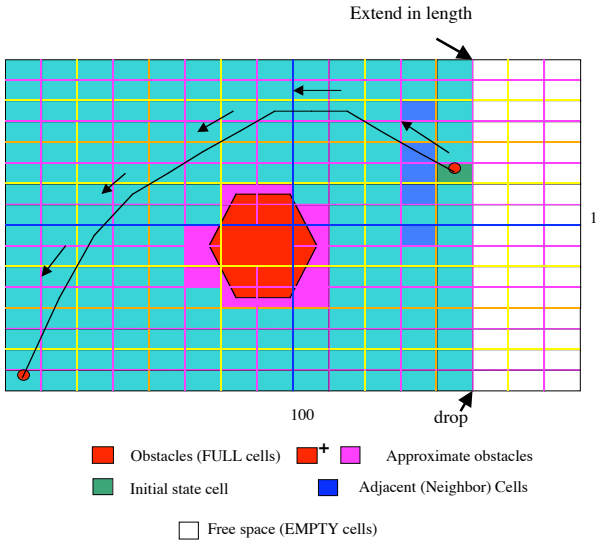

Fig. 5 Example search space for modified cell decomposition.

B. Search/Optimization Strategy

Once the cell decomposition map is created, this space must be explored to identify the optimal trajectory given landing site boundary condition (x_f, y_f, V_f) and approach entry constraints ($x_{\min}$, $y_{\min}$, V_0). Given our discrete search space and global optimization requirement, candidate algorithms include dynamic programming and A* search,[18] with an A* approach selected for this work due to its use of a best-first search to minimize number of expanded search states. A* explores nodes in best-first ordering based on an evaluation function *f(n)*. Let *g(n)* be the actual path cost from the start node (initial state X_i) to current node *n*, and let *h*(*n*) be the estimated cost of the cheapest path from n to the goal. The overall evaluation function *f(n) = g(n) + h(n)*, and it can be proven that A* yields an optimal result so long as h(n) is an admissible heuristic (i.e., never overestimates cost from current node to the final state). With *h(n)*>0, A* search is "informed" thus is typically more efficient in finding the optimal path. Given the complexity of the cost function, an admissible non-zero heuristic has not been identified thus the trajectory optimizer utilizes the search with $h = 0$ and *g(n)* set to the cost function described below. (In fact, when *h(n) = 0*, the search is the same as uniform-cost search with evaluation function *f(n) = g(n)*. The A* search procedure for our work is shown in Fig. 7. The set of search *nodes* is constructed during **Build**, 'u' is the current node being expanded, and 'c' is the cost from 'u' to an adjacent successor node 'w'. The current optimal path to each node can be reconstructed from the *parent* list.

The Modified Cell Decomposition algorithm is a global optimization technique. However, the solution is "optimal" only with respect to the level of discretization when dividing the continuous space into cells. Theoretically, this error can approach zero with infinite quad-tree depth level (resolution); however, computational complexity and path complexity also increases with depth level. We have wrapped an *iterative deepening strategy*[18] around the **Build** and **Search** algorithms to identify optimal solutions for each quad-tree depth level from 1-*n*. Initial low-depth solutions are simple (few segments) but may be costly. Higher-depth solutions approach the globally-optimal cost but will contain numerous flight segments that could only be feasible as SNI NAPs if a trusted autopilot capable of tracking these detailed trajectories is used. The iterative deepening procedure is shown in Fig. 8. In our work, we halt at a quad-tree depth where the difference between current and last cost is within a user-defined threshold ε. In practice, the pilot/airspace planner can break the loop manually to obtain intermediate solutions obtained from lower quad-tree depth levels.

This research is primarily geared toward the *offline* design of NAPs for RIA. For this purpose, the iterative deepening approach provides airspace planners with a solution set, i.e. one solution per quad-tree depth level. The iterative deepening approach, however, can also provide a real-time cockpit SNI NAP planning tool, acting as an anytime[19] algorithm that quickly provides simple (low-depth) routes when necessary but offers lower-cost (high-depth) solutions given sufficient computation time.

V. Cost Function

Traditional trajectory synthesis tools permit optimization over fuel and/or time. Pilot or airline preferences and air traffic control constraints contribute to the relative importance (weight) of these two optimization factors. NAP design requires an additional noise cost function term, the relative importance of which can be varied with time/fuel by varying relative weighting factors. Since fixed-wing airspace "obstacles" are considered impenetrable in this work, they are specifically excluded from the search space rather than modeled in the cost function. If this constraint were relaxed, for example, in cases where fully SNI routes did not exist due to the number and size of fixed-wing corridors, the search-space may be extended "inside" obstacles and fixed-wing airspace intersection penalties would then factor into cost.

For the SNI airspace design work presented in this paper, the cost function (f = *g(n)*) for trajectory optimization is given by

$$f = c_1 \int_{t_0}^{t_i} 10^{P/10} dt + c_2 \left(t_i - t_0 \right) + c_3 m_{fuel,i} + c_4 \dot{\gamma} \tag{6}$$

In this expression, t_0 is the initial state time, t_i is the current time at state *i*, $m_{fuel,i}$ is the total fuel consumed up to state *i* in Eq. (2). BVI noise, given by the empirical expression for P in Eq. (4), is integrated over the flight path in Eq. (5). Transient maneuvers resulting in non-zero $\dot{\gamma}$ and acceleration are governed by vehicle dynamics and will affect all cost function terms in Eq. (6). ($\dot{\gamma}$ over a transient maneuver from segment *i* to *k* is computed as $(\gamma_i - \gamma_k)/\Delta t$. In our case, Δt is set to 1 second.) Because $\dot{\gamma}$ also reflects passenger comfort and is not specifically considered in our quasi-static BVI noise model, we include a distinct $\dot{\gamma}$ cost term. Coefficients $c_1 - c_4$ may be adjusted based on relative prioritization of time, fuel, noise, and rejection of flight path excursions $\dot{\gamma}$.

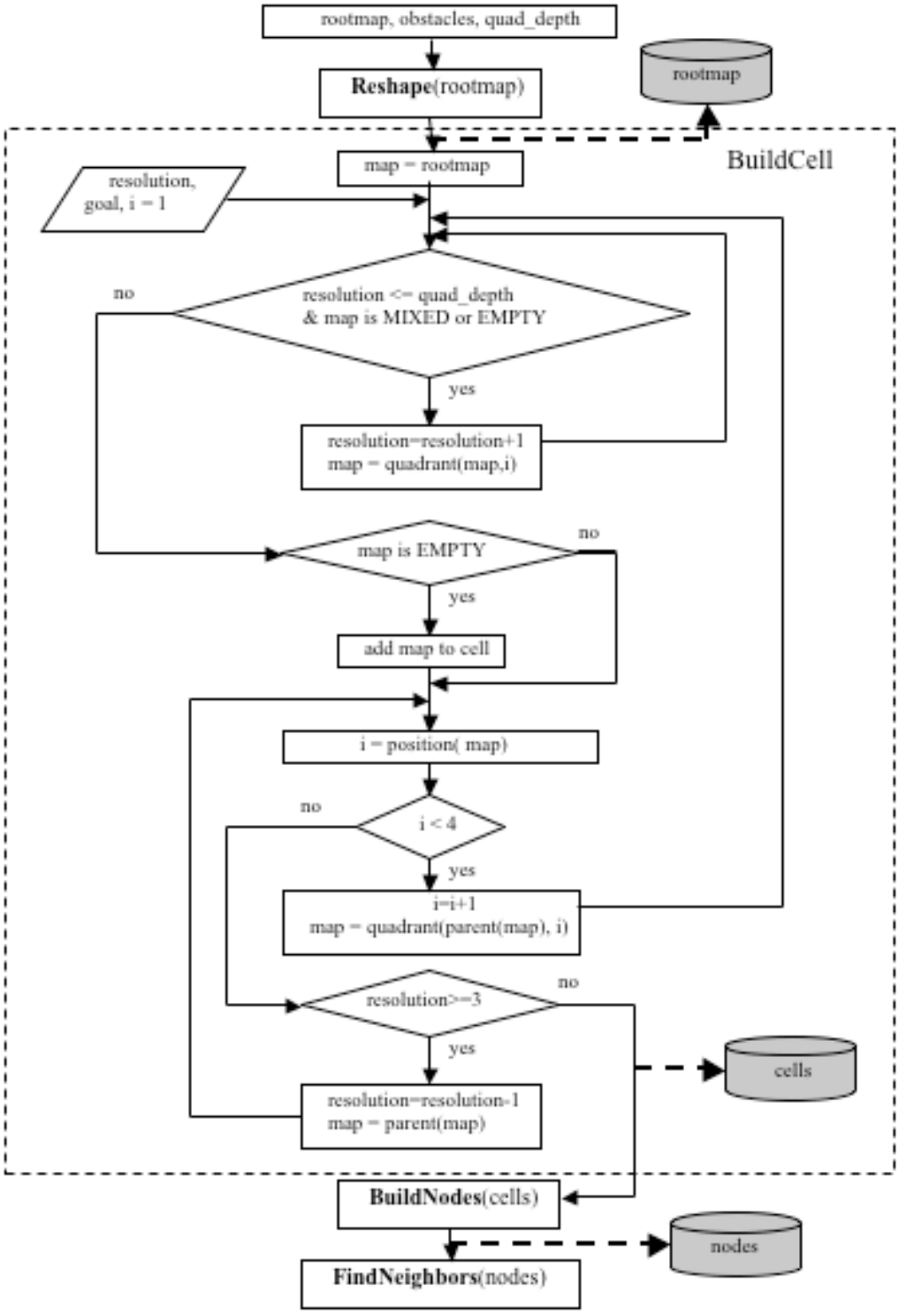

Fig. 6 Build algorithm.

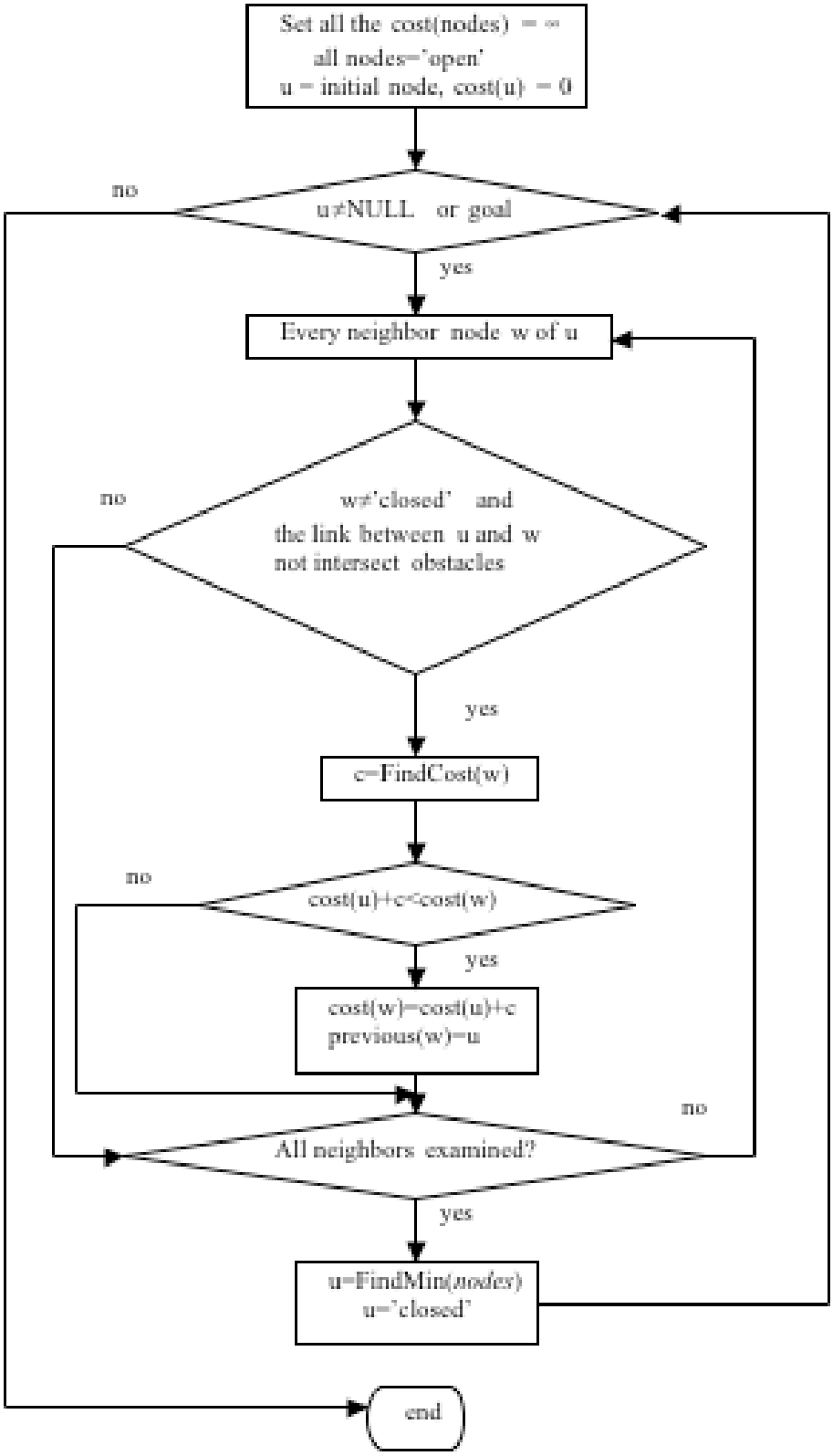

Fig. 7 Search algorithm.

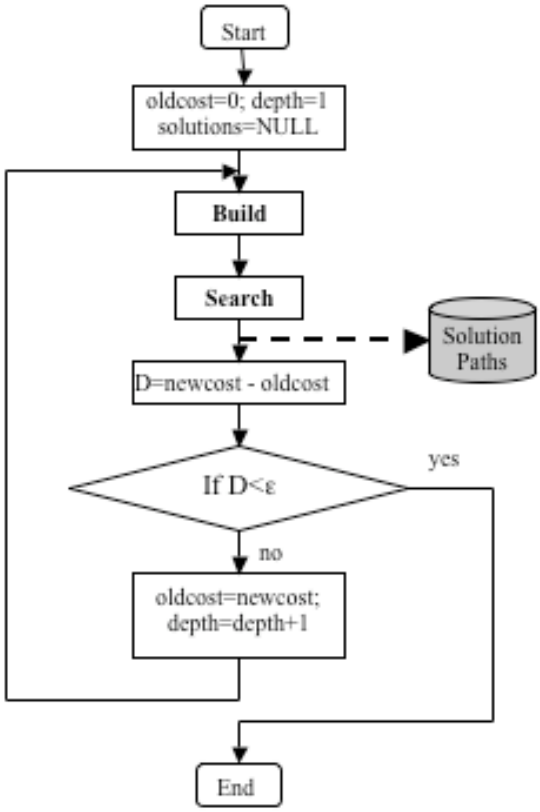

Fig. 8 Iterative deepening anytime algorithm for real-time trajectory generation.

VI. Optimization Results

To identify SNI NAP characteristics and study the effects of cost function parameters, the modified cell decomposition algorithm was applied to the design of final approach trajectories. These results are intended to provide insight regarding the use of the optimization tool and associated cost function to adjust SNI NAP characteristics. Once specific RIA landing sites and fixed-wing traffic patterns (airspace use) have been identified, this tool can be applied to specific rather than hypothetical cases. For all presented examples, the FATO area boundary is defined as x = 50 ft, altitude y = 10 ft, and the approach entry area is constrained by x>40,000 feet and y>2,000 feet. To remain within the valid Q-SAM region from which our noise model was derived,[4] a minimum altitude constraint y>50 ft was also imposed. Presented results are organized to disambiguate the effects of each cost term as well as search-space discretization (quad-tree depth) level. Unless otherwise stated, presented results utilize a quad-tree depth level of 6, generally observed to provide sufficient optimization resolution without introducing unreasonable path complexity. The first cases illustrate optimal trajectory properties when only noise is minimized (c_1=1;c_2=c_3=0), with and without the flight path excursion penalty (c_4). Next, optimal time-fuel approach trajectories are reviewed (c_1=c_4=0; c_2=c_3=1). A comparison between noise and time/fuel optimality is explored, followed by an analysis of the tradeoff between simple (real-time, low quad-tree depth) and optimal (high resolution) solutions.

A. BVI Noise Only

Typical of a helicopter approach, consider a case in which initial velocity is 95 knots and final velocity is 45 knots. The resulting optimal “bang-bang” solution is a sequence of accelerated climbs and decelerating descents (Fig. 9). This result maximizes the distance of the wake from the rotor, thereby minimizing vortex-induced noise. Fig. 9 also illustrates the worst-case (maximum noise) approach, during which wake and rotor blade are minimally separated. When optimizing only over BVI noise, the minimum-cost solution oscillates between accelerating climbs and decelerating descents within the specified boundary constraints.

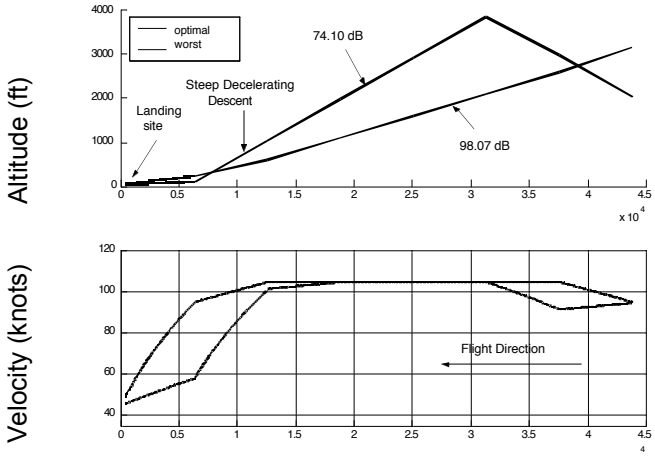

Fig. 9 Optimal and worst-case approaches from 95 knots to 45 knots.

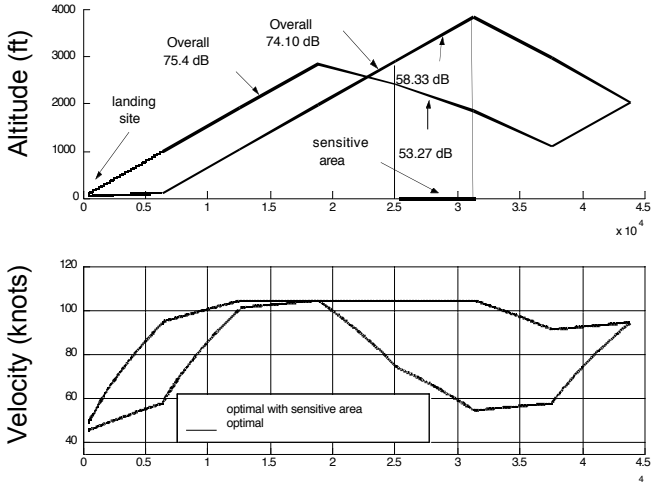

Fig. 10 Optimal SNI approach with extra noise penalty over sensitive region.

In practice, certain residential communities may be more noise sensitive than other commercial use or unpopulated regions. In this case, cost function weight c_1 can be assigned such that noise-sensitive segments incur higher penalty than less-sensitive areas. Consider an example in which a noise-sensitive area exists under the final approach path between ~25,000 and 32,000 ft from touchdown. With higher weight on this segment, the optimal solution (Fig. 10) chooses an accelerating climb during the noise-sensitive segment, generating ~5dB less noise per unit time than the noise-optimal solution with uniform c_1.

The SNI NAP optimization procedure was next applied with a single intersecting airspace obstacle to illustrate the effects of intersecting fixed-wing airspace corridors. This obstacle is modeled as a polygon that approximates the perpendicular intersection of the longitudinal SNI final approach plane with a cylindrical three-dimensional fixed-wing airspace corridor of radius 300 ft. As illustrated by Fig. 11, when the globally-optimal solution lies within such an obstacle, the resulting solution is the minimum of alternative local minima from the unobstructed longitudinal plane or neighboring sub-optimal solutions adjacent but exterior to the obstacle. The particular choice depends on the nature of the objective function in the neighborhood of the optimal solution. If the objective function remains relatively constant when perturbed about the optimal solution, a neighboring sub-optimal solution may be preferred (Fig. 11). Otherwise, one of the numerous other locally-optimal solutions that exhibit large flight path excursions and do not intersect the obstacle would be selected.

The previous example illustrates the fundamental effect of an airspace obstacle on optimal trajectory. In practice, multiple airspace corridors may intersect the RIA final approach plane, and in the limit, no feasible SNI solution

may exist. In this case, airspace planners must assess the tradeoff between coordinating RIA and fixed-wing traffic versus imposing fixed-wing route restrictions to free airspace for exclusive SNI use by the RIA. This planning tool can assist with such analysis, facilitating rapid SNI NAP construction for a variety of different airspace use cases.

B. BVI Noise & dγ/dt Cost Study

Figure 12 shows the noise-optimal solution for a constant speed approach with additional penalty on $\dot{\gamma}$, imposed for passenger comfort and because the quasi-static acoustic model does not include additional noise generated by $\dot{\gamma}$ transitions. In this case, c_4 is set to $6.4*10^8$ to approximately balance the numerically-large noise level (in pressure) with $\dot{\gamma}$. (Due to the discrete search space, the optimal solution is influenced only by significantly increasing c_4. The c_4 values listed in this paper were chosen to impact but not dominate overall cost. For comparison, Fig. 12 also indicates the optimal trajectory without the $\dot{\gamma}$ penalty, indicating that a significant reduction in flight path angle transition results in a noise level increase of less than 1 dB. Recall that our best single-segment NAP (Case V in Table 1) had 77.0dB noise level, slightly less than the analogous cell decomposition solution (78.2dB in Fig. 12) due to the limited altitude (ceiling) in our cell map.

Figure 13 extends the original BVI noise case (Fig. 9) to a quad-tree depth level of 7. After exploring a series of relative cost weights, coefficient c_4 is set to $2.5*10^5$. The resulting solution reduces flight path excursions with one less "bang-bang" transition between extrema, while the noise has increased only 0.03 dB. If c_4 is further increased to $1.7*10^6$, the path has only a single bang-bang transition with an additional 0.05 dB. In both cases the bang-bang solution with c_4 =0 is provided as a reference.

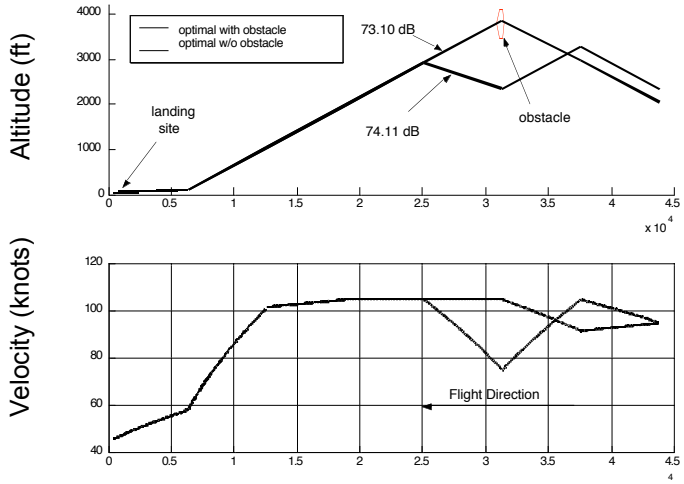

Fig. 11 Optimal SNI approach from 95 to 45 knots with a single airspace obstacle.

C. Time & Fuel Cost Study

As expected, approach duration primarily depends on aircraft speed, with secondary effect from flight path angle transitions that perturb trajectory length. Quite simply, a time cost penalty drives the optimizer to select the highest possible approach speed. As described previously (Fig. 1), a fuel penalty will drive an optimal path to follow a "best-glide" speed during approach and also favors the maximum descent angle for gravity-assist speed maintenance. However, since the case study from this paper enforces maximum and minimum speed constraints of 105 knots and 38 knots, respectively, both time and fuel penalties drive the solution toward a maximum-velocity, best-glide trajectory from initial to final states, as shown in Fig. 14. Under the velocity constraints the optimal result first accelerates to the maximum possible speed (V_{max}), which is maintained until a final maximum-deceleration (-0.05g) maneuver matches final state velocity (45 knots). As a comparison, Fig. 14 also depicts the worst case, in which an initial climb and deceleration to minimum velocity result in maximum fuel and time cost. If an airspace obstacle constraint is imposed along the optimal path, the resulting solution, a global minimum for the specified boundary constraints is an adjacent solution with maximum speed and overall descent angle.

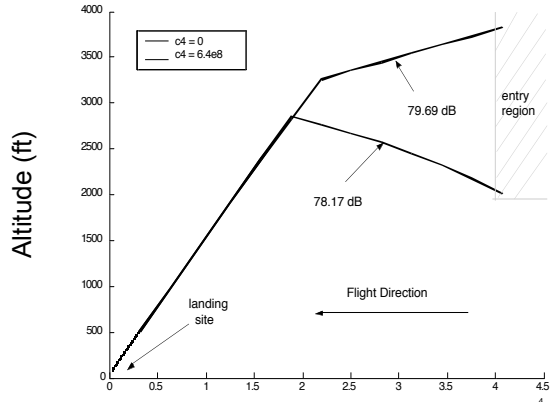

Fig. 12 Constant speed (70 knots) optimal approach path with and without $\dot{\gamma}$ penalty

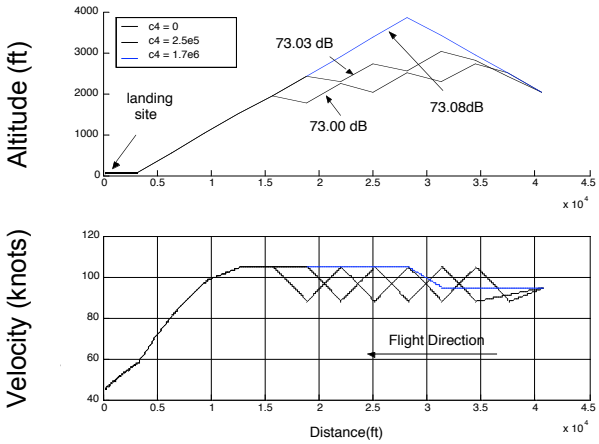

Fig. 13 Approach from 95 knots to 45 knots for varied c_4.

D. Noise & Time/Fuel Trade Study

From previous discussion, it may be observed that the optimal time/fuel path is similar to the worst-case shallow descent trajectory for BVI noise, while the optimal BVI noise trajectory increases time and fuel usage. The final SNI NAP solution must therefore balance noise with time and fuel. To simplify this tradeoff and gain insight for the final approach case studied in this work, the cost function is further simplified as Eq. (7). Because the time and fuel optimal solutions are similar given the approach velocity constraints, only the simple flight time cost is incorporated. To disambiguate the tradeoff between noise and time/fuel cost, the effect of $\dot{\gamma}$ is not included.

$$f = \int_{t_0}^{t_i} 10^{P/10} dt + \eta * (t_i - t_0) \tag{7}$$

where $\eta = c_2/c_1$. Figure 15 illustrates optimal path cost as a function of η, while Table 2 provides the corresponding cost values. From the comparison, it may be observed that, since the minimum-noise path has high velocity even though the path profile appears worst-case for time/fuel, the time/fuel actually consumed is significantly better than the real worst-case. However, there is still a significant efficiency difference, particularly if integrated over numerous flight operations. Figure 16 illustrates the tradeoff between a low-noise, high time/fuel solution (low η) and a high-noise, low time/fuel solution (high η). As shown in the figure, noise cost is primarily minimized until η increases to ~10^6. Within the interval [10^7, 10^{10}], dominance transitions until the time cost term is drives the optimization process. By selecting a coefficient η within this transition region (e.g., highlighted cases B or C in

Table 2), a solution acceptable in noise, time, and fuel may be identified. Note that the time and fuel cost terms are similar but not identical, as illustrated by minimum fuel use in Table 2 for $\eta=10^6$ rather than higher values. This supports the presence of both time and fuel terms in the full cost function in Eq. (6).

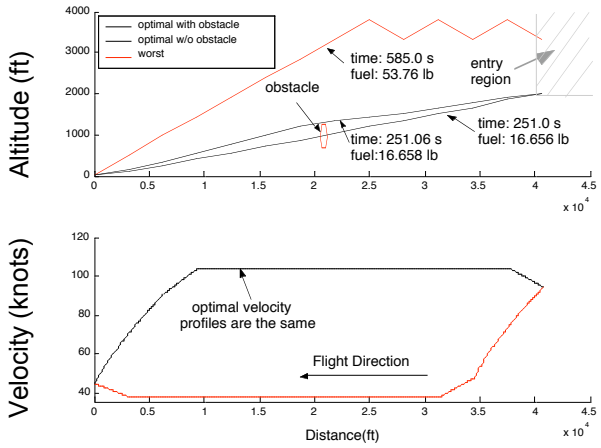

Fig. 14 Minimum and maximum cost path based on time/fuel cost.

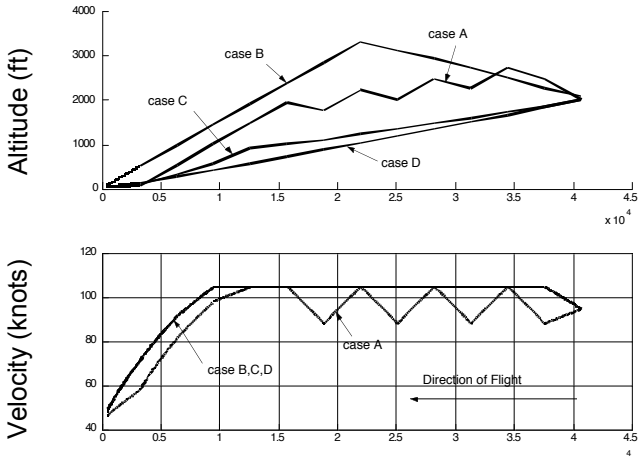

Fig. 15 Optimal approach solutions as a function of η.

Table 2 Optimal Solution Cost as a Function of η.

Case	η	Noise (SEL_{av}) (dB)	Time (s)	Fuel (lb)
A	0	73.0	275.42	18.247
B	$\mathbf{10^6}$	**73.57**	**259.81**	**16.28**
C	$\mathbf{10^7}$	**76.67**	**252.59**	**16.471**
D	10^{10}	90.03	251.097	16.66

E. Iterative Deepening Solution Set

Use of the iterative deepening search strategy provides a suite of optimal solutions, one for each quad-tree depth level. Figure 17 provides an example solution path set with only the noise cost term, while Table 3 provides quad-tree depth, total number of flight segments, average completion time when executed under Linux on a 1GHz Pentium III, and NAP cost for each of the five generated solutions. Figure 17 illustrates the increasing trajectory complexity as depth is increased. For Case 1 (depth=3), a single-segment solution is identified. Note that the high cost results from the constant deceleration from 95 to 45 knots that requires the trajectory to pass through the BVI peak noise region. Case 2 extends well beyond the 40,000 ft distance constraint, leveraging an initial accelerating climb to reduce overall noise. Cases 3 and 4 couple a single accelerating climb with a decelerating descent, providing reasonable 74-76dB NAPs with moderate complexity. Case 5 minimizes noise with thirteen flight segments, providing a low-cost but undesirable "bang-bang" flight trajectory. The Case 1-3 solution set is typically generated in less than 20 seconds, providing a potential real-time noise abatement flight trajectory-planning tool that could be implemented in the cockpit even before the RIA concept is realized.

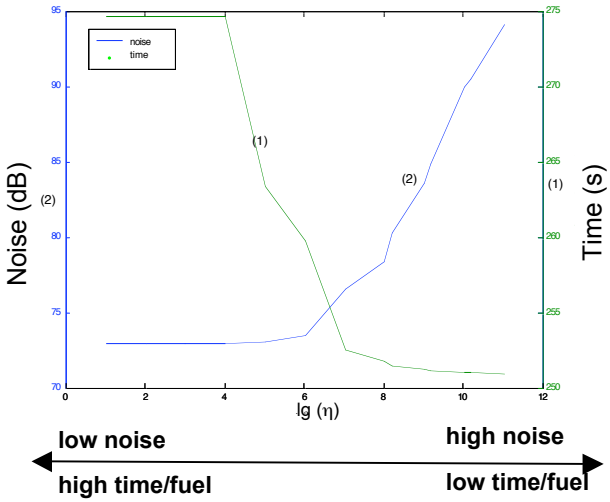

Fig. 16 Optimal trajectory noise and fuel as a function of η.

Table 3 Noise-optimal solution cost with increasing depth level

Case	Quad-Tree Depth	Flight Segments	Average Exec. Time (s)	Ground Noise (dB)
1	3	1	<<1	88.60
2	4	3	3	80.27
3	5	4	8	76.59
4	6	7	146	74.10
5	7	13	1756	73.00

VII. Conclusions and Future Work

An approach for optimizing segmented simultaneous non-interfering (SNI) noise abatement procedures (NAP) for runway-independent aircraft (RIA) has been presented. Fixed-wing airspace corridors are treated as impenetrable obstacles, and trajectories are optimized with respect to radiated noise, fuel, and time. A modified cell decomposition algorithm is combined with a uniform-cost search strategy to generate an optimal solution that meets

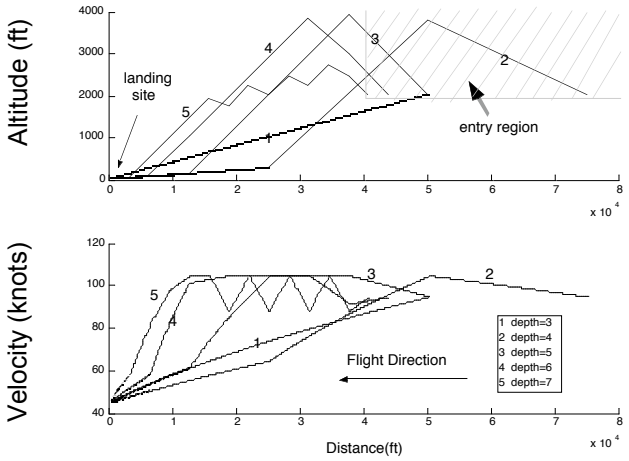

Fig. 17 Noise-optimal approaches from 95 to 45 knots as a function of quad-tree depth.

aircraft dynamic constraints. Optimal final approach trajectories for an AH-1 helicopter are generated using an empirical model of BVI noise derived from the test-validated Q-SAM (quasi-static acoustic model). These trajectories exhibit several interesting characteristics. A noise-optimal rotorcraft trajectory alternates accelerating climbs and decelerating descents to the landing site at maximum $|\gamma| = 9^\circ$ to avoid the peak BVI noise region. Airspace obstacles force the optimal SNI trajectory to a sub-optimal solution exterior but adjacent to the obstacle or, in some cases, to a very different path corresponding to a local minimum from the unobstructed longitudinal plane. A $\dot{\gamma}$ penalty smoothes the trajectory, which otherwise is a bang-bang solution to minimize noise alone. Increased noise cost penalty over noise-sensitive communities (as in Fig. 10) biases the trajectory to perform an accelerating climb over the sensitive region to reduce BVI noise. (Future inclusion of engine noise may switch this preference to a decelerating descent that avoids peak BVI noise.) A clear tradeoff between noise and time/fuel efficiency exists, enabling the user to balance the relative weighting factors (as in Table 2) to build a low-noise, efficient trajectory. The iterative deepening search strategy serves two purposes: it provides an anytime algorithm for approximate solution computation in real-time, and it generates progressively more complex segmented trajectories that can be compared with the simpler solutions to tradeoff trajectory complexity with reduction in noise, time, and fuel cost.

The presented examples were intended to provide intuitive understanding of trajectory characteristics as a function of cost weights and path complexity. If the trajectory is constrained to a single segment to minimize pilot workload, noise and time/fuel efficiency considerations favor a 9° descent with constant mid-range (e.g., 70 knot) velocity to avoid peak BVI noise. A multi-segment trajectory facilitates computation of SNI routes and is capable of meeting any feasible final velocity constraint at minimum cost when globally optimized.

Translation of optimal final approach *trajectories* into noise abatement *procedures* is straightforward. Each segment s_i of n-segment procedure $P = \{s_1, s_2, \ldots, s_n\}$ is fully-specified as the tuple $s_i = \langle \gamma_i, V_i, \dot{V}_i \rangle$ with $\dot{V}_i = 0$ for constant velocity and $V_i = undef$ for constant acceleration. If a mixed fleet of RIA vehicle classes emerges (e.g., rotorcraft and eSTOL), different NAPs may be required, with a rotorcraft (for example) executing an accelerating climb–decelerating descent profile just ahead of an eSTOL aircraft executing strictly a low-thrust decelerating descent. Air traffic automation aids analogous to those under development for fixed-wing decelerating descent approaches[8] will be required to sequence RIA traffic. Note that the RIA traffic can be sequenced without consideration of fixed-wing traffic queues provided SNI procedures are in effect.

If an airport terminal area has a fixed route structure, detailed SNI NAPs could be computed offline and published as a reference for pilots and ATC. If, on the other hand, dynamic terminal routing is present, a NAP planner must identify low-cost paths in real-time, and a true SNI NAP planner for RIA must circumvent dynamic fixed-wing routes selected independent of RIA operations. Realistically, with dynamic routing, the RIA traffic would collaboratively define its route, potentially given lower priority value than fixed-wing traffic.

Future work will concentrate on extending the noise model and optimization algorithm to three-dimensions and applying them to alleviate congestion at overcrowded urban airports. Final approach trajectories will likely remain two-dimensional to minimize workload and enable an aligned visual approach except for brief diversions around extremely noise-sensitive communities. However, determination of full SNI terminal area routes will certainly

require three-dimensional flight, and work is underway to extend the current cell decomposition model and reduce the search space such that additional computational complexity is minimized. As data becomes available, realistic models of fixed-wing airspace obstacles and potential stub runway landing sites will be generated for select urban airports. Real-time traffic and noise simulations will be performed to evaluate throughput improvements versus ground noise penalties. Alternatively, if this research finds that true SNI corridors cannot be generated for crowded airspace regions (e.g., Newark/JFK/LaGuardia), the "impenetrable obstacle" constraint will necessarily be relaxed or modified. Currently, rotorcraft traffic is manually sequenced by terminal area controllers. The low-noise SNI trajectory generation tools developed for this research may also be incorporated into next-generation ATC software to formally define rotorcraft-specific approach/departure procedures at airports with frequent VTOL operations.

Due to its well-understood properties, near-term research will continue with a rotorcraft model for general RIA airspace corridor design; however, it is unclear whether public acceptance and efficiency concerns will support rotorcraft as a viable alternative air transportation vehicle. Work is underway to develop an acoustic and performance model for an eSTOL aircraft, with plans to incorporate its dynamic constraints, performance model, and noise characteristics into the SNI trajectory optimizer to provide a more comprehensive airspace design tool.

References

[1]Newman, D., and Wilkins, R., "Rotorcraft Integration into the Next Generation NAS," *Proceedings of the American Helicopter Society (AHS) 54th Annual Forum*, May 1998.

[2]Clarke, J.-P., "Systems Analysis of Noise Abatement Procedures Enabled by Advanced Flight Guidance Technology," *Journal of Aircraft*, Vol. 37, No. 2, pp. 266-273, March-April 2000.

[3]Johnson, W., *Helicopter Theory*, Dover Publications, New York, 1994.

[4]Gopalan, G., Xue, M., Atkins, E., and Schmitz, F., "Longitudinal-Plane Simultaneous Non-Interfering Approach Trajectory Design for Noise Minimization", *Proceedings of the American Helicopter Society (AHS) 59th Annual Forum*, May 2003.

[5]Gopalan, G., Schmitz, F. H., and Sim, B. W., "Flight Path Management and Control Methodology to Reduce Helicopter Blade-Vortex (BVI) Noise," *Proceedings of the American Helicopter Society (AHS) Vertical Lift Aircraft Design Conference*, Jan. 2000.

[6]Elmer, K., Wat, J., Shivashankara, B., Clarke, J.-P., Tong, K., Brown, J., and Warren, A., "Community Noise Reduction using Continuous Descent Approach: A Demonstration Flight Test at Louisville," *Proceedings of the 9th AIAA/CEAS Aeroacoustics Conference and Exhibit*, AIAA Paper 2003-3277, May 2003.

[7]Gershzohn, G., Wat, J., Dwyer, J., Elmer, K., Clarke, J.-P., and Ho, N. T., "Advanced Noise Abatement Procedures: An Experimental Study of Flight Operational Acceptability," *Proceedings of the 2nd AIAA Aircraft, Technology, Integration, and Operations Forum*, AIAA Paper 2002-5867, Oct. 2002.

[8]Ho, N. T., and Clarke, J.-P., "Mitigating Operational Aircraft Noise Impact by Leveraging on Automation Capability," *Proceedings of the 1st AIAA Aircraft, Technology, Integration, and Operations Forum*, AIAA Paper 2001-5239, Oct. 2001.

[9]Betts, J. T., "Survey of Numerical Methods for Trajectory Optimization," *Journal of Guidance, Control, and Dynamics*, Vol. 21, 1998.

[10]Seywald, H., Cliff, E., and Well, K., "Range Optimal Trajectories for an Aircraft Flying in the Vertical Plane," *Journal of Guidance, Control, and Dynamics*, Vol. 17, 1994.

[11]Schultz, R.L., "Three-Dimensional Trajectory Optimization for Aircraft," *Journal of Guidance, Control, and Dynamics*, Vol. 13, 1990.

[12]Hagelauer, P., "Contribution a l'Optimisation Dynamique de Trajectoires de Vol pour un Avion de Transport," Ph.D. Dissertation, CNRS - Universite Paul Sabater de Toulouse, France, June 1997.

[13]Slattery, R. and Zhao J., "Trajectory Synthesis for Air Traffic Automation," *Journal of Guidance, Control, and Dynamics*, Vol. 20, 1997.

[14]Vormer, F. J., Mulder M., van Paassen, M. M., and Mulder, J., "Design and Preliminary Evaluation of a Segment-based Routing Methodology," *Proceedings of the AIAA Guidance, Navigation, and Control Conference*, AIAA Paper 2002-4861, Aug. 2002.

[15]Latombe, J.-C., *Robot Motion Planning*, Kluwer Academic Press, 1991.

[16]Beard, R., McLain, T., Goodrich, M., and Anderson, E., "Coordinated Target Assignment and Intercept for Unmanned Air Vehicles," *IEEE Transactions on Robotics and Automation*, Vol. 18, No. 6, Dec. 2002.

[17]Brooks, R.A., and Lozano-Perez, T. "A Subdivision Algorithm in Configuration Space for Findpath with Rotation," *Proceedings of the 8th International Conference on Artificial Intelligence*, 1983, pp. 799-806.

[18]Russell, S., and Norvig, P., *Artificial Intelligence: a Modern Approach*, Prentice Hall Series, New Jersey, 1995.

[19]Dean, T., Kaelbling, L. P., Kirman, J., and Nicholson, A., "Planning under Time Constraints in Stochastic Domains," *Artificial Intelligence*, Vol. 76, Nos. 1-2, 1995, pp. 35-74.